

Conservative Time Discretization: A Comparative Study

Marcelo Forets¹[0000-0002-9831-7801] and
Christian Schilling²[0000-0003-3658-1065]

¹ DMA, CURE, Universidad de la República, Uruguay
mforets@gmail.com

² Aalborg University, Aalborg, Denmark
christianms@cs.aau.dk

Abstract. We present the first review of methods to overapproximate the set of reachable states of linear time-invariant systems subject to uncertain initial states and input signals *for short time horizons*. These methods are fundamental to state-of-the-art reachability algorithms for long time horizons, which proceed in two steps: First they use such a method to discretize the system for a short time horizon, and then they efficiently obtain a solution of the new discrete system for the long time horizon. Traditionally, both qualitative and quantitative comparison between different reachability algorithms has only considered the combination of both steps. In this paper we study the first step in isolation. We perform a variety of numerical experiments for six fundamental discretization methods from the literature. As we show, these methods have different trade-offs regarding accuracy and computational cost and, depending on the characteristics of the system, some methods may be preferred over others. We also discuss preprocessing steps to improve the results and efficient implementation strategies.

Keywords: Time discretization · Linear system · Reachability

1 Introduction

We study the fundamental problem of reachability for a system of linear differential equations. Given a set of initial states $\mathcal{X}_0 \subseteq \mathbb{R}^n$, we are interested in the set of states that can be reached by any trajectory up to some time horizon.

The classical analysis approach is numerical simulation, which has several drawbacks. First, one can only simulate finitely many trajectories, but a system has infinitely many trajectories. Second, a simulated trajectory is only available at finitely many discrete points in time. Third, even for these discrete points in time, a standard simulation is not guaranteed to be exact. For all these reasons, simulation may miss critical behaviors, which can lead to wrong conclusions.

In contrast, reachability algorithms construct a finite sequence of *sets* covering *all* possible *continuous* trajectories of the system. In general it is not possible to represent the exact set of reachable states, but for linear systems one can obtain arbitrary-precision approximations as a union of convex sets [26,5].

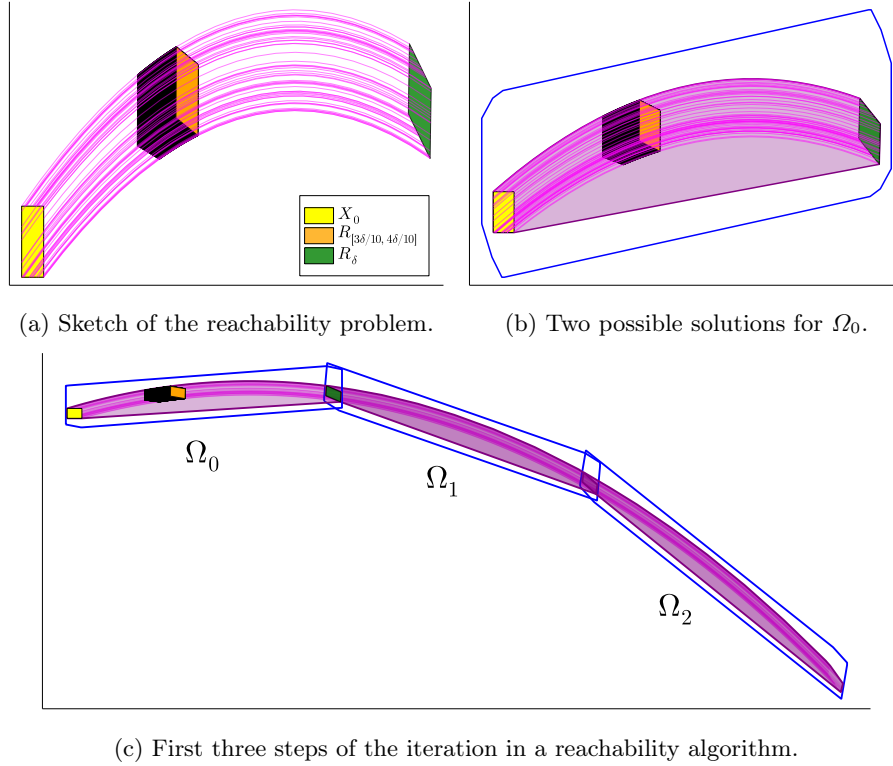


Fig. 1: **Left:** Starting from the initial states \mathcal{X}_0 (yellow), we want to enclose the states reachable within $[0; \tau]$, $\mathcal{R}_{[0,\delta]}$, covering the random trajectories (magenta). **Right:** The purple set is the smallest convex solution for Ω_0 . The blue set is a zonotope solution for Ω_0 computed with the method in [8]. **Bottom:** The first three sets of the discretized system computed by a reachability algorithm.

The fundamental procedure behind all modern reachability algorithms [4] consists of two stages. In the first stage, the system is discretized, i.e., approximated by a discrete system. This requires to find a Euclidean set $\Omega_0 \subseteq \mathbb{R}^n$ that includes all states reachable starting from any initial state $x(0) \in \mathcal{X}_0$ up to a small time horizon τ , as illustrated in Fig. 1(a). Two possible solutions for Ω_0 are presented in Fig. 1(b). In the second stage, the set Ω_0 is propagated forward in time until the time horizon is reached, which is sketched in Fig. 1(c). Thus computing a precise Ω_0 is important for the precision of the overall result.

All state-of-the-art reachability tools such as CORA [2], the continuous version of Hylaa [11], HyPro [29], JuliaReach [12], and SpaceX [19] follow this procedure of discretizing and computing an approximation Ω_0 . Over the years, multiple methods to obtain such sets Ω_0 have been proposed [15,10,20,8,26,19,13,3]. These methods are tailored toward different set representations as a requirement

of the second stage of the reachability algorithm. The two prevalent options are a concrete representation with a zonotope and a lazy representation based on the support function. Nevertheless, the different sets \mathcal{R}_0 solve the same problem and can be partially interchanged between different algorithms. However, to our knowledge, these methods have never been compared to each other.

In this article we study different methods to compute \mathcal{R}_0 . We introduce this problem formally in the next section. Our study has these particular goals:

- Present the methods in a unified way (Section 3).
- Discuss potential gains of system transformations (Section 4).
- Discuss aspects of an efficient implementation (Section 5).
- Assess the effect of different system characteristics and evaluate the methods on different systems (Section 6).

2 Problem statement

In this work we study linear time-invariant (LTI) systems, which have the state-space form

$$\dot{\mathbf{x}}(t) = \mathbf{A}\mathbf{x}(t) + \mathbf{u}(t); \quad (1)$$

where \mathbf{x} is an n -dimensional state vector, $\mathbf{A} \in \mathbb{R}^{n \times n}$ is the flow matrix, and \mathbf{u} is a bounded but arbitrarily varying input signal that belongs to the input domain $\mathcal{U} \subseteq \mathbb{R}^n$, i.e., $\mathbf{u}(t) \in \mathcal{U}$ for all $t \geq 0$. It is common to associate a linear map \mathbf{B} with \mathbf{u} in (1), but this map can be absorbed in \mathcal{U} (via $\mathcal{U} \mapsto \mathbf{B}\mathcal{U}$, which is no restriction in practice because common set representations for \mathcal{U} such as zonotopes are closed under linear maps). An LTI system is homogeneous if $\mathcal{U} = \{0\}$ and heterogeneous otherwise. We consider initial-value problems for system (1) where the initial state $\mathbf{x}(0) \in \mathbb{R}^n$ is taken from a set of initial states $\mathcal{X}_0 \subseteq \mathbb{R}^n$. The solution of (1) for a particular initial state \mathbf{x}_0 and input signal \mathbf{u} is the trajectory $x_{0,u}(t)$, which is a function of time. The set of solutions at time t is the set of reachable states

$$\mathcal{R}_t = \{ x_{0,u}(t) : \mathbf{x}_0 \in \mathcal{X}_0; \mathbf{u} \in \mathcal{U} \}; \quad (2)$$

and we generalize this set to time intervals

$$\mathcal{R}_{[t_0, t_1]} = \{ x_{0,u}(t) : \mathbf{x}_0 \in \mathcal{X}_0; \mathbf{u} \in \mathcal{U}; t \in [t_0; t_1] \}; \quad (3)$$

The time-bounded reachability problem asks to compute the set of reachable states $\mathcal{R}_{[0, T]}$ up to a time horizon T . Solving this problem exactly for LTI systems is generally not possible [24]. Hence an overapproximation $\mathcal{R}_0 \supseteq \mathcal{R}_{[0, T]}$ is sought in practice. The common approach to compute the set \mathcal{R}_0 proceeds in two stages.

In the first stage, conservative time discretization is applied to compute a set \mathcal{R}_0 with the property that it encloses the exact reachable states for an initial time interval $[0; \delta]$, i.e., $\mathcal{R}_0 \supseteq \mathcal{R}_{[0, \delta]}$; usually one chooses a small value for δ , much smaller than T . We illustrate two possible choices for \mathcal{R}_0 in Fig. 1(b).

For efficiency reasons, in practice one restricts \mathcal{X}_0 to convex sets. Under this restriction, the smallest set \mathcal{X}_0 is the convex hull of $\mathcal{R}_{[0,\delta]}$ (purple set in Fig. 1(b)).

In a similar fashion to \mathcal{X}_0 , the second stage also requires a discretized input set \mathcal{V} , which encloses the trajectories of system (1) but starting from the origin ($\mathbf{x}(0) = 0$), up to the time horizon T . Since the set \mathcal{U} is often assumed to have a simple shape, the computation of \mathcal{V} is straightforward and mostly identical across the different discretization methods, and we do not discuss it further.

The second stage propagates the set \mathcal{X}_0 through consecutive time intervals until reaching the time horizon T , which we sketch briefly because the technicalities are not of interest. The sequence of sets \mathcal{X}_k , $k \geq 0$, is given by the following recurrence, where \oplus denotes the Minkowski sum, $\mathcal{X} \oplus \mathcal{Y} = \{\mathbf{x} + \mathbf{y} : \mathbf{x} \in \mathcal{X}; \mathbf{y} \in \mathcal{Y}\}$:

$$\mathcal{X}_k = e^{A\delta k} \mathcal{X}_0 \oplus \bigoplus_{j=0}^{k-1} e^{A\delta j} \mathcal{V} \quad (4)$$

We finally define our approximation of the reachable states (see Fig. 1(c)) as

$$= \bigcup_{k=0} \mathcal{X}_k \quad (5)$$

We note that state-of-the-art reachability algorithms for LTI systems are wrapping-free, i.e., they do not accumulate errors over time; as such, the precision of these algorithms is mainly determined by the precision of \mathcal{X}_0 and \mathcal{V} .

The reader may wonder why reducing the problem of computing $\mathcal{X}_0 \supseteq \mathcal{R}_{[0,T]}$ to the problem of computing $\mathcal{X}_0 \supseteq \mathcal{R}_{[0,\delta]}$, which is structurally equivalent, makes sense. It is important to remark that there are good convex approximation methods for small enough values of δ , but these methods fail for large values of δ (as we shall see later). While \mathcal{X}_0 is convex, \mathcal{X}_k is a union of convex sets (and thus typically not convex). We also note the analogy to numerical simulation methods, which may also require that the time step is small enough, for instance by the well-known Courant-Friedrichs-Lewy condition.

In summary, the fundamental problem that we study here is:

Problem 1. Given an LTI system and a time horizon T , find a set $\mathcal{X}_0 \supseteq \mathcal{R}_{[0,\delta]}$.

3 Discretization methods

In this section, after fixing some common notation and mentioning approaches for nonlinear systems, we introduce various methods to obtain a conservative discretization \mathcal{X}_0 for solving Problem 1. The presentation follows the chronological order in which these methods have been proposed. The methods for computing \mathcal{X}_0 we consider here assume that \mathcal{X}_0 and \mathcal{U} are at least compact and convex. Under this condition it is known that \mathcal{R}_t is also compact and convex for any t (unlike the sets $\mathcal{R}_{[t_1,t_2]}$). We end the section with pointers to related works outside the scope of this study.

3.1 Notation

In this article, when the norm of an operator is not specified, we assume a p -norm with $1 \leq p \leq \infty$. We denote the ball of radius ϵ in some p -norm and centered in the origin by \mathcal{B}_ϵ , and \mathcal{B}_ϵ^p when the p -norm is relevant. Let $\mathcal{X}, \mathcal{Y} \subseteq \mathbb{R}^n$ be sets. The norm of \mathcal{X} is defined as $\|\mathcal{X}\| = \sup_{x \in \mathcal{X}} \|x\|$. The symmetric interval hull of \mathcal{X} , written $\square(\mathcal{X})$, is the smallest hyperrectangle that contains \mathcal{X} and is centrally symmetric in the origin. We write $CH(\mathcal{X}; \mathcal{Y})$ to denote the convex hull of the union of \mathcal{X} and \mathcal{Y} , and $\sigma(\mathbf{d}; \mathcal{X})$ to denote the support function of \mathcal{X} along direction $\mathbf{d} \in \mathbb{R}^n$ (see for instance [17] for a formal definition and examples). Given system (1), we define the state-transition matrix $\Phi = e^{A\delta}$ as the matrix exponential of A . The following matrix function is also relevant:

$$\mathcal{I}_2(A; \delta) = \sum_{i=0}^{\infty} \frac{\delta^{i+2}}{(i+2)!} A^i; \tag{6}$$

If A is invertible, $\mathcal{I}_2(A; \delta) = A^{-2}(\delta^2 I - \delta A)$. See Section 5.2 for the computation.

3.2 Methods for nonlinear systems

In principle, we can apply reachability algorithms for nonlinear systems to LTI systems as a special case. However, the methods developed specifically for LTI systems are much more precise and scalable. Hence we do not include nonlinear approaches in our study and only briefly mention some relevant works below.

A polyhedral enclosure \mathcal{R}_0 can be computed for any dynamical system by choosing a set of normal directions $(\mathbf{d}_i)_i$ and solving the corresponding optimization problems $\max_{t \in [0, \delta]} \mathbf{d}_i^T \mathbf{x}(t)$ [15]. This scheme relies on a sound optimizer and the run time depends on the number of directions and is difficult to predict. For LTI systems, the analytic expression of $\mathbf{x}(t)$ can be used [25, Section 5.3].

The work in [9], describes how to deal with nondeterministic inputs for Lipschitz-continuous systems. If L is the Lipschitz constant, the reachable states of the heterogeneous system are contained in the bloated reachable states of the homogeneous system: $\mathcal{R}_{heterog} \subseteq \mathcal{R}_{homog} \oplus \mathcal{B}_\epsilon$, where $\epsilon = \frac{\|\mathcal{U}\|}{L}(e^{L\delta} - 1)$.

3.3 Common structure of methods for linear systems

Examining the different methods that we study in the remainder of this section, the following common structure emerges:

$$\mathcal{R}_0 = CH(\mathcal{X}_0; \mathcal{X}_0 \oplus \mathcal{H}) \oplus \mathcal{J}; \tag{7}$$

for suitable sets \mathcal{H} and \mathcal{J} (possibly empty). In short, the idea is to compute the convex hull between the reachable states at time 0 and at time δ , \mathcal{X}_0 and \mathcal{X}_δ . That would suffice if the trajectories were just following straight lines. To correct for the curvature, the bloating terms \mathcal{H} and \mathcal{J} need to be added.

3.4 First-order d/dt method

The earliest work specifically designed for linear systems we are aware of was developed for the tool d/dt [10]. This work only considers homogeneous systems. The definition is

$$\mathcal{X}_0 = CH(\mathcal{X}_0; \mathcal{X}_0) \oplus \mathcal{B}_\varepsilon; \quad (8)$$

where

$$\varepsilon = \left(e^{\|\mathbf{A}\|\delta} - 1 - \|\mathbf{A}\| \right) \|\mathcal{X}_0\| - \frac{3}{8} \|\mathbf{A}\|^2 \|\mathcal{X}_0\|; \quad (9)$$

We note that the authors also claim that their method can be used to obtain an underapproximation, but this is not correct (see Appendix C for details).

3.5 First-order zonotope method

The work in [20] computes a zonotope enclosure. The idea is to cover $CH(\mathcal{X}_0; \mathcal{X}_0)$ with a zonotope and then bloat with another zonotope (here: a ball in the infinity norm):

$$\mathcal{X}_0 = \text{zonotope}(CH(\mathcal{X}_0; \mathcal{X}_0)) \oplus \mathcal{B}_\varepsilon^\infty \quad (10)$$

where

$$\varepsilon = \left(e^{\|\mathbf{A}\|_\infty \delta} - 1 - \|\mathbf{A}\|_\infty \right) \left(\|\mathcal{X}_0\|_\infty + \frac{\|\mathcal{U}\|_\infty}{\|\mathbf{A}\|_\infty} \right) + \|\mathcal{U}\|_\infty; \quad (11)$$

3.6 Correction-hull method

The method in [8] is designed for interval dynamics matrix \mathbf{A} , which represents uncertain parameters and has the scalar matrix as a special case. The resulting set, a zonotope, is constructed from interval linear maps, which is described in [8, Theorem 4]. The approach is based on truncating the Taylor series at a chosen order p , and this order must satisfy the following inequality:

$$\frac{\|\mathbf{A}\|_\infty}{p+2} < 1; \quad (12)$$

The method assumes that the input domain \mathcal{U} contains the origin. If this is not the case, a simple transformation can bring the system to this form [1, Section 3.2.2], which we describe in Section 4.1. Then we have the following definitions:

$$\mathcal{X}_0 = CH(\mathcal{X}_0; \mathcal{X}_0) \oplus \mathbf{F}_p \mathcal{X}_0 \oplus \mathbf{G}_p \mathcal{U}; \quad (13)$$

where the correction matrices \mathbf{F} and \mathbf{G} are

$$\mathbf{F}_p = \mathbf{E} + \sum_{i=2}^p \left[{}^i(i-1) - i \binom{i-1}{i-1}; 0 \right] \frac{\mathbf{A}^i}{i!} \quad (14)$$

and

$$\mathbf{G}_p = \mathbf{E} + \sum_{i=0}^p \frac{\mathbf{A}^{i+1}}{(i+1)!}; \quad (15)$$

The remainder matrix \mathbf{E} to bound $\sum_{i=p+1}^{\infty} \mathbf{A}^{i+1}$ is a diagonal interval matrix based on results in [27]; here the assumption (12) is relevant to make the geometric series $\sum_i \mathbf{A}^{i+1}$ converge. Define

$$\mathbf{E} = [-\alpha; \alpha] \mathbf{1} \quad (16)$$

where $\mathbf{1}$ is the $n \times n$ matrix filled with ones and

$$\alpha = \frac{(\|\mathbf{A}\|_{\infty})^{p+1}}{(p+1)!} \frac{1}{1 - \|\mathbf{A}\|_{\infty}}; \quad (17)$$

The method was later extended in [7] and in our implementation we use the remainder term \mathbf{E} from that work instead.

3.7 First-order method

The method in [26] uses a first-order approximation similar to [20] in Section 3.5, but in contrast it is not restricted to zonotopes and the infinity norm:

$$\mathcal{X}_0 = CH(\mathcal{X}_0; \mathcal{X}_0 \oplus \mathcal{U} \oplus \mathcal{B}_{\varepsilon}) \quad (18)$$

where

$$\alpha = \left(e^{\|\mathbf{A}\|\delta} - 1 - \|\mathbf{A}\|\delta \right) \left(\|\mathcal{X}_0\| + \frac{\|\mathcal{U}\|}{\|\mathbf{A}\|} \right); \quad (19)$$

3.8 Forward-backward method

The approach in [19] describes an optimization procedure similar in spirit to the one discussed in Section 3.2 but specialized for LTI systems. Here one only needs to optimize over a quadratic function. First we define some auxiliary terms.

$$\mathbf{E}_+ = \square(\alpha \|\mathbf{A}\|; \alpha \|\mathbf{A}\|) \square(\mathbf{A}^2 \mathcal{X}_0) \quad (20)$$

$$\mathbf{E}_- = \square(\alpha \|\mathbf{A}\|; \alpha \|\mathbf{A}\|) \square(\mathbf{A}^2 \mathcal{X}_0) \quad (21)$$

$$\mathbf{E}_{\psi} = \square(\alpha \|\mathbf{A}\|; \alpha \|\mathbf{A}\|) \square(\mathbf{A} \mathcal{U}) \quad (22)$$

$$\mathcal{Y}_{\lambda} = (1 - \lambda) \mathcal{X}_0 \oplus \lambda \mathcal{X}_0 \oplus \mathcal{U} \oplus (\mathbf{E}_+ \cap (1 - \lambda) \mathbf{E}_-) \oplus \lambda \mathbf{E}_{\psi}$$

Here the term \mathbf{E}_+ goes forward from \mathcal{X}_0 and the term \mathbf{E}_- goes backward from \mathcal{X}_0 , and it is sufficient to consider their intersection. The solution is then obtained by optimizing \mathcal{Y}_{λ} (where the objective function is piecewise-linear for homogeneous systems and piecewise-quadratic for heterogeneous systems):

$$\mathcal{X}_0 = CH\left(\bigcup_{\lambda \in [0,1]} \mathcal{Y}_{\lambda}\right); \quad (23)$$

3.9 Forward-only method

The work in [13] uses a simplified version of (23) with only a forward approximation, which works without an optimization procedure. It can be seen that

$$CH\left(\bigcup_{\lambda \in [0,1]} \mathcal{Y}_\lambda\right) \subseteq CH(\mathcal{Y}_0; \mathcal{Y}_1 \oplus \mathbf{E}_+) \quad (24)$$

and this method accordingly uses

$$\mathbf{x}_0 = CH(\mathcal{X}_0; \mathcal{X}_0 \oplus \mathcal{U} \oplus \mathbf{E}_\psi \oplus \mathbf{E}_+); \quad (25)$$

where \mathbf{E}_+ and \mathbf{E}_ψ are defined in (20) and (22). Analogously one can define a “backward-only” method by using \mathbf{E}_- instead of \mathbf{E}_+ .

3.10 Combining methods

It should be noted that if \mathbf{x}_0^a and \mathbf{x}_0^b are two solutions to Problem 1, then their intersection $\mathbf{x}_0^a \cap \mathbf{x}_0^b$ is also a solution. (The dual statement holds for under-approximations and their unions.) It is hence possible to combine the different methods outlined above. This idea was used in [16] where the authors combined the “forward-only” method with the mentioned “backward-only” method; this method yields solutions that are closer to the “forward-backward” method than these methods individually but is more efficient than the latter.

3.11 Application to high-dimensional systems

The approach in [3] shows how to efficiently work with high-dimensional systems. The construction of \mathbf{x}_0 is similar to the “correction-hull” method, including the focus on zonotopes as set representation. The difference is that the structure of the solution is rewritten to rely on matrices in the Krylov subspace. The idea is to compute two matrices W and H to approximate the effect of a vector v on the matrix exponential e^A without computing it:

$$e^A v \approx \|v\| W e^H \mathbf{e}_1; \quad (26)$$

The matrix exponential e^H can be computed efficiently, and there exist estimates to bound the above approximation error [3].

In [16] the authors demonstrated that the “forward-only” method can also be efficiently implemented with Krylov techniques.

3.12 Application to time-varying systems

Linear systems whose dynamics are time-varying due to uncertain parameters can be represented with interval matrices. This setting differs from the one in [8] from Section 3.6 where the system dynamics are uncertain but time-invariant. Methods based on zonotopes to handle such systems are presented in [1,6].

4 Problem transformations

In this section we shortly explain possible transformations of system (1) to a normal form. These transformations are simple but yield interesting results.

For illustration, we use a simple harmonic oscillator with inputs f ,

$$\ddot{y}(t) + \omega^2 y(t) = f; \tag{27}$$

where $\omega^2 = 4$, $m = 1$ and $y(t)$ is the unknown. This problem can be associated with a spring-mass system, where $y(t)$ is the elongation of the spring at time t and ω is the natural frequency. Bringing Eq. (27) to the first-order form of Eq. (1) with the change of variables $x(t) = [y(t); \dot{y}(t)]^T$, we obtain

$$\dot{x}(t) = \begin{pmatrix} 0 & 1 \\ -4 & 0 \end{pmatrix} x(t) + \begin{pmatrix} 0 \\ f \end{pmatrix}; \tag{28}$$

4.1 Homogenization

The first transformation, which was used in [1, Section 3.2.2] for the “correction-hull” method (although with a different goal) and in [16], expresses some of the inputs’ effect with a fresh state variable. For deterministic systems (i.e., where the input domain \mathcal{U} is a singleton), this allows to completely eliminate the inputs. For proper nondeterministic systems, this extracts the “central” effect of the input signals into a state variable and only leaves the deviation from this central effect, effectively re-centering the input domain \mathcal{U} in the origin. The transformation is motivated because \mathcal{U} is treated rather pessimistically in the methods to compute ρ_0 (e.g., it may appear in the form of its norm $\|\mathcal{U}\|$).

We illustrate the issue in one dimension. For the p -norms considered here and any $a \in \mathbb{R}$ we have $\|a\| = \|-a\|$. Hence the norm of the singleton $\mathcal{U}_1 = \{a\}$ is equivalent to the norm of the proper interval $\mathcal{U}_2 = [-a; a]$. Thus ρ_0 is identical in both cases, but since it must cover the \mathcal{U}_2 case, with many more possible behaviors, it is coarse for \mathcal{U}_1 and large a .

Now suppose that the input domain \mathcal{U} is centrally symmetric but not centered in the origin. The idea of the transformation is to shift \mathcal{U} to the origin and add another state variable to account for this shift. Formally, assume a heterogeneous system (1), an initial set \mathcal{X}_0 , and a domain \mathcal{U} centered in a point $c \neq 0$. We define a new system $\dot{y}(t) = Cy(t) + u(t)$, where we have the block matrix

$$C = \begin{pmatrix} A & \frac{b}{\alpha} \\ 0 & 0 \end{pmatrix} \tag{29}$$

for some value $\alpha \neq 0$, $\mathcal{Y}_0 = \mathcal{X}_0 \times \{c\}$ is the new initial set, and $\mathcal{U} \oplus \{-c\}$ is the new input domain. The parameter α can be used to trade off the impact in the norm of C (for methods where this term appears) and \mathcal{Y}_0 . This transformation increases the state dimension n by one and removes the input dimension. The modification of the initial states (i.e., the construction of \mathcal{Y}_0 from \mathcal{X}_0) is efficient for typical

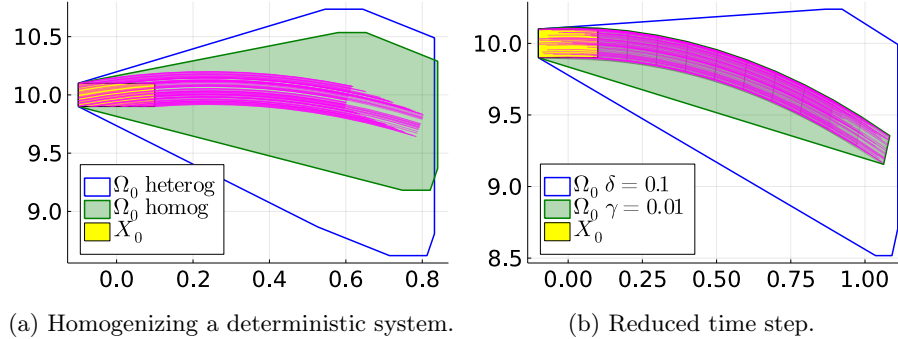


Fig. 2: **Left:** Several trajectories and the sets Ω_0 for a deterministic heterogeneous system (blue) and for the (projected) homogenized system (green). **Right:** Several trajectories and the sets Ω_0 obtained with a time step $\delta = 0:1$ (blue) and obtained by first computing the sets $\Omega'_0; \dots; \Omega'_k$ with a time step $\gamma = 0:01$ (light gray, below the trajectories) and then computing the convex hull of their union (green). We use the “forward-only” method in all cases.

set representations of \mathcal{X}_0 . Likewise, projecting away the auxiliary dimension in the end is efficient for common set representations since this dimension is independent of all other dimensions and has the constant value 1.

It is easy to see that the set of trajectories of the latter system, after projecting away the auxiliary dimension, is equivalent to the set of trajectories of the original system. Yet, discretization methods typically yield more precise results for the latter system. We illustrate this claim in Fig. 2(a) for the deterministic harmonic oscillator. The effect for nondeterministic systems is almost identical and is shown in Fig. 8 in Appendix D.

4.2 Shrinking the time step

The time step δ has a large impact on the precision of Ω_0 . Recall that Ω_0 is convex while $\mathcal{R}_{[0,\delta]}$ is generally not, so we have $\Omega_0 \supseteq CH(\mathcal{R}_{[0,\delta]}) \supseteq \mathcal{R}_{[0,\delta]}$. The gaps between these three sets grow with larger δ . Indeed, most methods have the property that they converge to $\mathcal{R}_{[0,\delta]}$ for $\delta \rightarrow 0$. The reason for not choosing a very small δ in practice is that the reachability algorithm requires $\lceil \frac{T}{\delta} \rceil$ steps to cover the time horizon T . Hence one needs to find a balance for δ : small enough to obtain a precise Ω_0 and large enough to be efficient later.

Observe that the gap between $CH(\mathcal{R}_{[0,\delta]})$ and $\mathcal{R}_{[0,\delta]}$ only depends on δ . Say that we fix δ to keep $\lceil \frac{T}{\delta} \rceil$ in a feasible range. The best we can do is minimize the gap between Ω_0 and $CH(\mathcal{R}_{[0,\delta]})$. We can achieve this by choosing a positive integer k and a smaller time step $\gamma = \delta/k$, computing the corresponding discretization Ω'_0 and propagating it (using some reachability algorithm) until time horizon T , which yields sets $\Omega'_0; \dots; \Omega'_{k-1}$, and finally constructing Ω_0 from their convex hull $CH(\Omega'_0 \cup \dots \cup \Omega'_{k-1})$. We illustrate this idea in Fig. 2(b).

5 Efficient implementation

As mentioned in Section 3.3, the different methods can be phrased in the structure of Eq. (7). Exceptions to this rule are the “first-order zonotope” method and the “forward-backward” method. The former applies an intermediate simplification to the CH, while the latter involves a CH in a continuous variable. In this section we describe how to operate with Eq. (7) numerically in an efficient way, even in high dimensions. We show example code for the set library `LazySets.jl`³ [17]. If we allow for a post-processing operation, all the discretization methods can be cast into the same symbolic-numeric framework. We briefly describe the user interface for the implementation of the discretization methods available in the library `ReachabilityAnalysis.jl`⁴ in Appendix B.

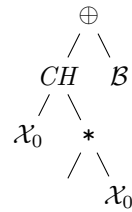
5.1 The concept of a lazy set

The key to an efficient implementation is lazy evaluation, that is, to *delay* computational effort until a result is needed. For example, we show how the “first-order d/dt” method from Section 3.4 can be implemented using `LazySets`, with the harmonic oscillator from Section 4 as running example. In this case, the sets \mathcal{H} and \mathcal{J} in Eq. (7) are the empty set and \mathcal{B}_ε , respectively. The following command defines the set Ω_0 as a lazy representation of Eq. (8).

```

1 # first-order d/dt method
2 julia> Ω₀ = CH(X₀, Φ*X₀) ⊕ B
    
```

In other words, the lazy set operations (Minkowski sum, convex hull, and linear map) are not evaluated. The execution is instantaneous, while obtaining a concrete representation such as a polyhedron scales with the dimension of the sets. The operations are internally represented in the form of a tree as shown in the diagram on the right. Further operations such as the support function, conversion, and approximation can be efficiently applied to that symbolic representation [17].



5.2 Computation of matrix functions

Some discretization methods require special matrix functions such as \exp_2 defined in Eq. (6). If A is not invertible, it can be obtained as the sub-matrix of the exponential of a higher-order matrix [19]. However, for large systems (typically $n > 2000$ depending on the sparsity pattern of A), such an approach can be prohibitively expensive. Instead, it is possible to use Krylov-subspace methods as discussed in Section 3.11, provided that we reformulate the problem as the action of a matrix function over a direction. To illustrate this point, consider the

³ See github.com/JuliaReach/LazySets.jl
⁴ See github.com/JuliaReach/ReachabilityAnalysis.jl

Table 1: Average run times (in seconds) for different heat model instances.

Model instance	HEAT01	HEAT02	HEAT03	HEAT04
# Mesh points	5^3	10^3	20^3	50^3
Forward	0.134	23.6	-	-
Forward & Krylov	0.001	0.004	0.07	1.367

“forward-only” from Section 3.9. Assume that the system is homogeneous and \mathcal{X}_0 is a hyperrectangle with center and radius vectors $\mathbf{c}; \mathbf{r} \in \mathbb{R}^n$ respectively. A priori, the Krylov method does not apply to Eq. (20) because \mathcal{H}_2 is acting on the set $H_{in} := \square(\mathbf{A}^2 \mathcal{X}_0)$. However, we observe that H_{in} is a hyperrectangle centered in the origin with radius $r_{in} = |\mathbf{A}^2 \mathbf{c}| + |\mathbf{A}^2 \mathbf{r}|$. Therefore, it suffices to compute $\mathcal{H}_2(|\mathbf{A}|; r_{in}) = \mathcal{H}_2(|\mathbf{A}|; |\mathbf{A}^2 \mathbf{c}| + |\mathbf{A}^2 \mathbf{r}|)$ using Krylov methods.

As an application, we consider the discretized heat partial differential equation model used in [4], whose details can be found in Appendix A. A run-time comparison is presented in Table 1. The non-Krylov implementation cannot handle the larger instances because the computation of the matrix exponential runs out memory. The Krylov method additionally offers a significant speedup.

5.3 Simplification of the set representation

It is possible to post-process the set Ω_0 with another set that makes it easier to operate with in reachability algorithms. For example, an approximation with an axis-aligned box can be used. The main advantage of such a representation is that the support function can be computed efficiently. This is shown in the following comparison when computing the support function of Ω_0 resp. its box approximation along direction $\mathbf{d} = (1; 1)^T$. The box approximation of Ω_0 has approximately the same support value, but the computation is 13x faster.

```

1 julia> boxΩ₀ = box_approximation(Ω₀);
2
3 julia> d = [1.0, 1.0];
4
5 julia> ρ(d, Ω₀)
6 10.328776223585699
7
8 julia> ρ(d, boxΩ₀)
9 10.35390370135613
10
11 julia> @btime ρ($d, $Ω₀)
12 97.762 ns (1 allocation: 80 bytes)
13
14 julia> @btime ρ($d, $boxΩ₀)
15 7.209 ns (0 allocations: 0 bytes)

```

Table 2: Average run times (in milliseconds) for the different methods.

Model	d/dt	Zonotope	Correction hull	First-order	Fwd/bwd	Forward
Oscillator	0.01	0.02	0.23	0.01	6.56	0.03
TDoF	0.03	0.05	0.51	0.01	6.17	0.06
ISS	–	32.99	4 701.20	25.93	657.80	476.96

6 Experimental evaluation

In this section we evaluate the discretization methods from Section 3 in two experiments.⁵ In the first experiment, we visually compare the sets \mathcal{X}_0 for variants of the harmonic oscillator (see Section 4). In the second experiment, we evaluate the methods on representative models while varying the time step δ . Next we describe the experimental setup, show the results, and finally discuss them.

6.1 Setup

We implemented the different methods (called here d/dt, Zonotope, Correction hull, First-order, Forward/backward, and Forward) in JuliaReach [12]. For matrix-exponential functionality we use [28]. For the correction-hull method we use the truncation order $p = 4$ (higher orders led to numerical errors for the biggest model). To plot results for the forward-backward method, one needs to choose a set of directions to evaluate the support function. In the plots we choose 30 uniform directions from the unit circle; we choose this high precision to show the theoretical power of the method, even if in practice this is rarely required. We obtained the results on a notebook with a 2.20 GHz CPU and 8 GB RAM.

6.2 Visual evaluation of varying parameters

We evaluate the methods on the harmonic oscillator for three different analysis and model parameters. In Fig. 3 we vary the step size δ . In Fig. 4 we vary the size of the initial set \mathcal{X}_0 . In Fig. 5 we vary the size of the input domain \mathcal{U} . The plots also show a tight approximation of the true reachable states. For homogeneous systems, the analytic solution at time t can be computed ($e^{At}\mathcal{X}_0$) and we show several sets \mathcal{R}_t (for uniformly chosen time points t from $[0; T]$) instead.

6.3 Quantitative evaluation by scaling δ

We run a quantitative analysis on the harmonic oscillator and two other models described in Appendix A. The latter represent challenging model classes: The second model, a two-degree-of-freedom system, has a system matrix A of large norm; this shows the corresponding sensitivity of the methods. The third model,

⁵ The scripts are available at [18].

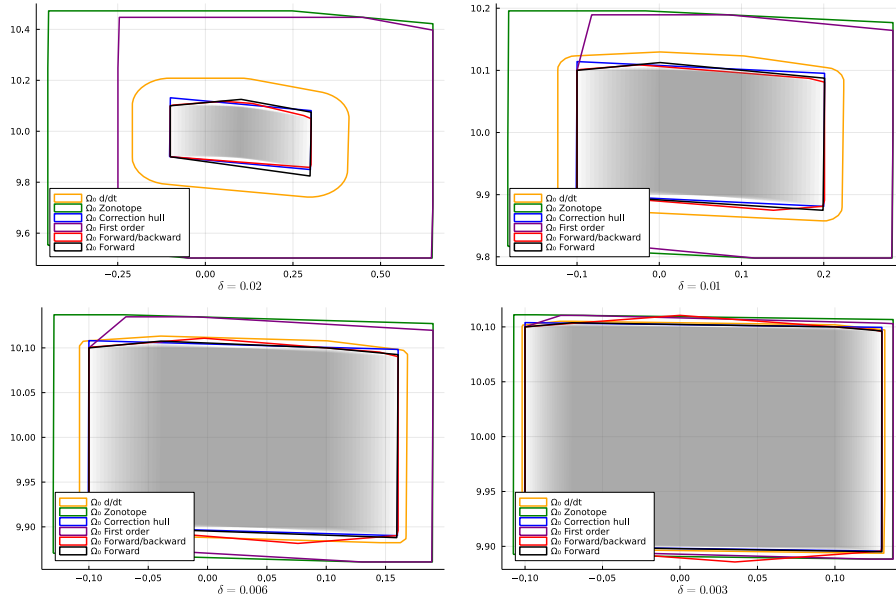


Fig. 3: The sets \mathcal{S}_0 obtained with different methods for varying values of δ . In gray we show \mathcal{R}_t for uniform $t \in [0; 1]$.

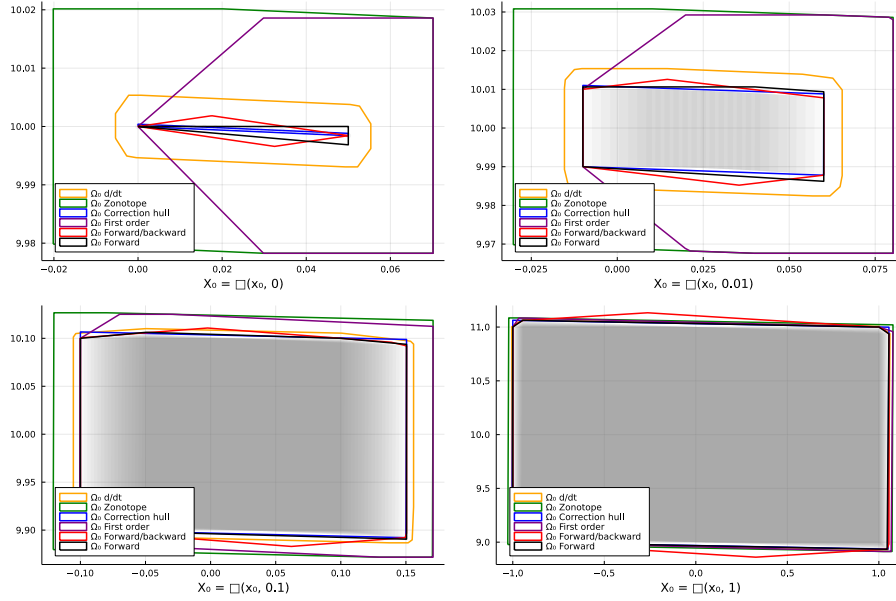


Fig. 4: The sets \mathcal{S}_0 obtained with different methods for $\delta = 0.005$ and varying sets X_0 . In gray we show \mathcal{R}_t for uniform $t \in [0; 1]$.

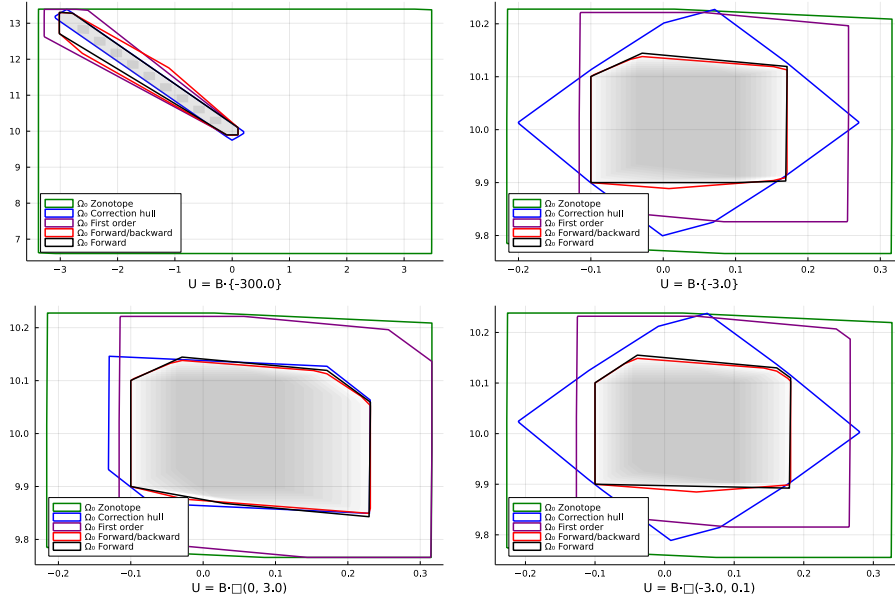


Fig. 5: The sets Ω_0 obtained with different methods for $\Delta t = 0:01$ and varying sets U . In gray we show \mathcal{R}_t for uniform $t \in [0; \cdot]$.

representing a docking maneuver at the International Space Station (ISS), is high-dimensional; this shows the scalability of the methods. For comparing the precision, we vary the time step Δt and compute the support function $(d; \Omega_0)$ of the sets Ω_0 in direction $d = (1; \dots; 1)^T$. The results are shown in Fig. 6. Average run times (which are independent of Δt) are given in Table 2. Note that Ω_0 is computed lazily except for the “zonotope” and the “correction-hull” methods.

6.4 Summary

We generally observe that the first-order methods (d/dt, Zonotope, First-order) yield coarser results and are more sensitive to the different model characteristics. In particular, for the two degree of freedom, a very small time step 10^{-5} is required to obtain precise results. This shows the sensitivity to the norm of A . The other three methods yield higher and similar precision, although the “correction-hull” method, which it is restricted to zonotopes, is generally incomparable (see for instance the first plot in Fig. 5). The “forward-backward” method is typically the most precise but also the most expensive method; recall that we computed a lazy representation of Ω_0 here and in a reachability application one needs to evaluate the support function of Ω_0 in multiple directions. The forward-only method is a simplification that yields a good compromise. The “correction-hull” method is much slower than the other methods for the largest model (ISS), but it computes a concrete zonotope. (Zonotopes enable an efficient “second stage”

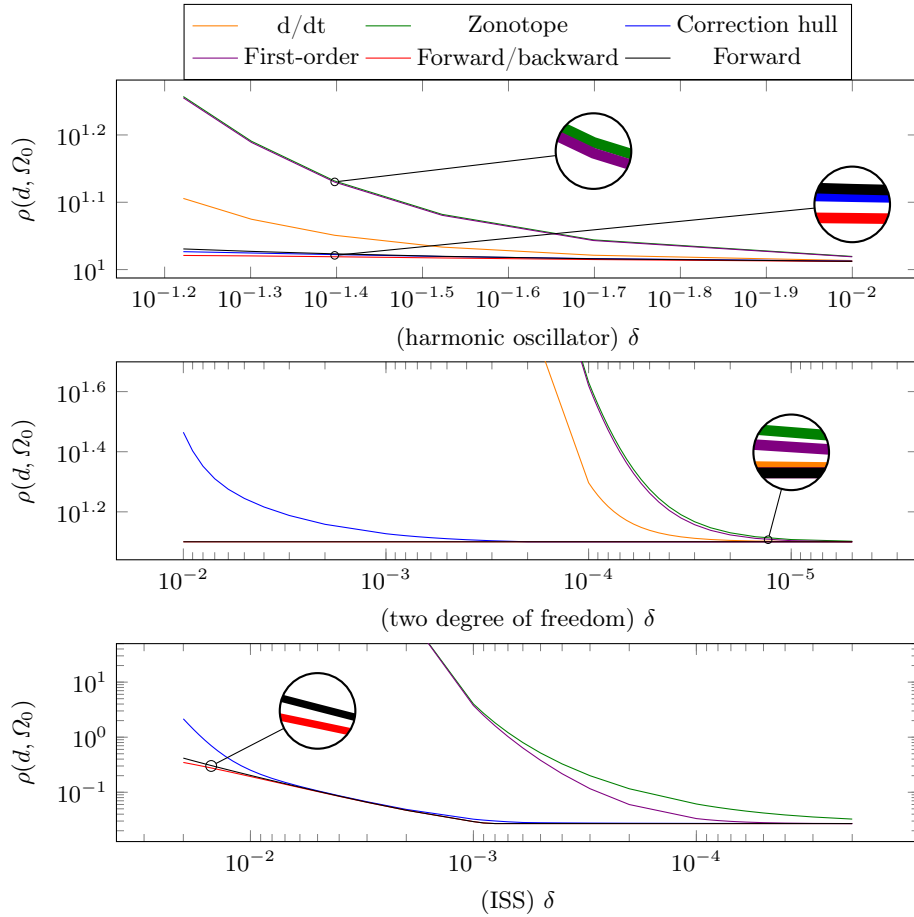


Fig. 6: Benchmark results with the graphs of $\rho(d; \Omega_0)$ (log axes). In the second plot, the methods “forward-backward” and “forward-only” yield identical results. In the third plot, the “d/dt” method is not applicable.

reachability analysis, which we ignore here.) Since this method is designed for interval matrices, it may be possible to devise a more efficient scalar variant.

7 Conclusion

In this article we have studied six methods for conservative time discretization. We have discussed potential ways to improve their output in practice and how to efficiently implement them. Our empirical evaluation shows that the methods have different characteristics. In particular, methods based on a first-order approximation are generally less precise than the other methods. In the future we plan to perform a similar study of the full-fledged reachability algorithms using the insights gained in this study to use a precise discretization model.

Acknowledgments This research was partly supported by DIREC - Digital Research Centre Denmark and the Villum Investigator Grant S4OS.

References

1. Althoff, M.: Reachability Analysis and its Application to the Safety Assessment of Autonomous Cars. Ph.D. thesis, Technische Universität München (2010)
2. Althoff, M.: An introduction to CORA 2015. In: ARCH. EPiC Series in Computing, vol. 34, pp. 120–151. EasyChair (2015). <https://doi.org/10.29007/zbkv>
3. Althoff, M.: Reachability analysis of large linear systems with uncertain inputs in the Krylov subspace. *IEEE Trans. Autom. Control.* **65**(2), 477–492 (2020). <https://doi.org/10.1109/TAC.2019.2906432>
4. Althoff, M., Ábrahám, E., Forets, M., Frehse, G., Freire, D., Schilling, C., Schupp, S., Wetzlinger, M.: ARCH-COMP21 category report: Continuous and hybrid systems with linear continuous dynamics. In: ARCH. EPiC Series in Computing, vol. 80, pp. 1–31. EasyChair (2021). <https://doi.org/10.29007/lhbw>
5. Althoff, M., Frehse, G., Girard, A.: Set propagation techniques for reachability analysis. *Annual Review of Control, Robotics, and Autonomous Systems* **4**(1), 369–395 (2020). <https://doi.org/10.1146/annurev-control-071420-081941>
6. Althoff, M., Guernic, C.L., Krogh, B.H.: Reachable set computation for uncertain time-varying linear systems. In: HSCC. pp. 93–102. ACM (2011). <https://doi.org/10.1145/1967701.1967717>
7. Althoff, M., Krogh, B.H., Stursberg, O.: Analyzing reachability of linear dynamic systems with parametric uncertainties. In: Modeling, Design, and Simulation of Systems with Uncertainties, pp. 69–94. Springer (2011). https://doi.org/10.1007/978-3-642-15956-5_4
8. Althoff, M., Stursberg, O., Buss, M.: Reachability analysis of linear systems with uncertain parameters and inputs. In: CDC. pp. 726–732. IEEE (2007). <https://doi.org/10.1109/CDC.2007.4434084>
9. Asarin, E., Dang, T., Girard, A.: Reachability analysis of nonlinear systems using conservative approximation. In: HSCC. LNCS, vol. 2623, pp. 20–35. Springer (2003). https://doi.org/10.1007/3-540-36580-X_5
10. Asarin, E., Dang, T., Maler, O., Bournez, O.: Approximate reachability analysis of piecewise-linear dynamical systems. In: HSCC. LNCS, vol. 1790, pp. 20–31. Springer (2000). https://doi.org/10.1007/3-540-46430-1_6
11. Bak, S., Tran, H., Johnson, T.T.: Numerical verification of affine systems with up to a billion dimensions. In: HSCC. pp. 23–32. ACM (2019). <https://doi.org/10.1145/3302504.3311792>
12. Bogomolov, S., Forets, M., Frehse, G., Potomkin, K., Schilling, C.: Juliareach: a toolbox for set-based reachability. In: HSCC. pp. 39–44. ACM (2019). <https://doi.org/10.1145/3302504.3311804>
13. Bogomolov, S., Forets, M., Frehse, G., Viry, F., Podelski, A., Schilling, C.: Reach set approximation through decomposition with low-dimensional sets and high-dimensional matrices. In: HSCC. pp. 41–50. ACM (2018). <https://doi.org/10.1145/3178126.3178128>
14. Chahlaoui, Y., Van Dooren, P.: Benchmark examples for model reduction of linear time-invariant dynamical systems. In: Dimension Reduction of Large-Scale Systems, pp. 379–392. Springer (2005). https://doi.org/10.1007/3-540-27909-1_24

15. Chutinan, A., Krogh, B.H.: Verification of polyhedral-invariant hybrid automata using polygonal flow pipe approximations. In: HSCC. LNCS, vol. 1569, pp. 76–90. Springer (1999). https://doi.org/10.1007/3-540-48983-5_10
16. Forets, M., Caporale, D.F., Zerpa, J.M.P.: Combining set propagation with finite element methods for time integration in transient solid mechanics problems. *Computers & Structures* **259** (2022). <https://doi.org/10.1016/j.compstruc.2021.106699>
17. Forets, M., Schilling, C.: LazySets.jl: Scalable Symbolic-Numeric Set Computations. *Proceedings of the JuliaCon Conferences* **1**(1), 11 (2021). <https://doi.org/10.21105/jcon.00097>
18. Forets, M., Schilling, C.: Package for repeatability evaluation (2022). <https://doi.org/10.5281/zenodo.6390631>, https://github.com/JuliaReach/iFM22_RE
19. Frehse, G., Guernic, C.L., Donzé, A., Cotton, S., Ray, R., Lebeltel, O., Ripado, R., Girard, A., Dang, T., Maler, O.: SpaceX: Scalable verification of hybrid systems. In: CAV. LNCS, vol. 6806, pp. 379–395. Springer (2011). https://doi.org/10.1007/978-3-642-22110-1_30
20. Girard, A.: Reachability of uncertain linear systems using zonotopes. In: HSCC. LNCS, vol. 3414, pp. 291–305. Springer (2005). https://doi.org/10.1007/978-3-540-31954-2_19
21. Han, Z., Krogh, B.H.: Reachability analysis of large-scale affine systems using low-dimensional polytopes. In: HSCC. *Lecture Notes in Computer Science*, vol. 3927, pp. 287–301. Springer (2006). https://doi.org/10.1007/11730637_23
22. Hughes, T.J.: *The finite element method: linear static and dynamic finite element analysis*. Courier Corporation (2012)
23. Koskela, A.: Approximating the matrix exponential of an advection-diffusion operator using the incomplete orthogonalization method. In: *Numerical Mathematics and Advanced Applications-ENUMATH 2013*, pp. 345–353. Springer (2015)
24. Lafferriere, G., Pappas, G.J., Yovine, S.: Symbolic reachability computation for families of linear vector fields. *J. Symb. Comput.* **32**(3), 231–253 (2001). <https://doi.org/10.1006/jsco.2001.0472>
25. Le Guernic, C.: Reachability analysis of hybrid systems with linear continuous dynamics. Ph.D. thesis, Université Joseph-Fourier-Grenoble I (2009)
26. Le Guernic, C., Girard, A.: Reachability analysis of linear systems using support functions. *Nonlinear Analysis: Hybrid Systems* **4**(2), 250–262 (2010). <https://doi.org/10.1016/j.nahs.2009.03.002>
27. Liou, M.L.: A novel method of evaluating transient response. *Proceedings of the IEEE* **54**(1), 20–23 (1966). <https://doi.org/10.1109/proc.1966.4569>
28. Rackauckas, C., Nie, Q.: DifferentialEquations.jl – a performant and feature-rich ecosystem for solving differential equations in Julia. *The Journal of Open Research Software* **5**(1) (2017). <https://doi.org/10.5334/jors.151>
29. Schupp, S., Ábrahám, E., Makhoulouf, I.B., Kowalewski, S.: Hypro: A C++ library of state set representations for hybrid systems reachability analysis. In: NFM. LNCS, vol. 10227, pp. 288–294 (2017). https://doi.org/10.1007/978-3-319-57288-8_20
30. Tran, H., Nguyen, L.V., Johnson, T.T.: Large-scale linear systems from order-reduction. In: ARCH. *EPiC Series in Computing*, vol. 43, pp. 60–67. EasyChair (2016). <https://doi.org/10.29007/xk7x>

A Model definitions

A.1 Heat3D

The linear Heat3D model is obtained from a spatial discretization of a partial differential equation for heat transfer in three dimensions. Originally presented in [21] for two dimensions and later extended to three dimensions, it was used as a benchmark example for reachability analysis [11,4]. The model dimension is scalable and here we consider four different instances of increasing complexity, which are labeled HEAT0x, for grids of size $n \times n \times n$ mesh points, i.e., the associated ODEs are n^3 -dimensional. The goal is to find the maximum temperature reached at the center of the spatially discretized domain, where one of its edges is initially heated. Since each mesh point corresponds to a given direction, it is sufficient to compute the support function along the center of the mesh. Furthermore, the set of initial states is a hyperrectangle contained in $[0; 1]^3$ and the matrix A is hermitian.

For the experiment described in Section 5.2 we use Krylov subspace dimension $m = 30$ for instance HEAT01 and $m = 100$ for the rest (see [23] for details).

A.2 Two degree of freedom

We consider a two-degree-of-freedom model from [22, Chapter 9]. The model has characteristics that are typical of large systems, containing both low-frequency and high-frequency components. It is given by

$$M\ddot{y}(t) + Ky(t) = 0; \quad y(t) = [y_1(t); y_2(t)]^T \quad (30)$$

where the mass (M) and stiffness (K) matrices are respectively

$$M = \begin{pmatrix} m_1 & 0 \\ 0 & m_2 \end{pmatrix}; \quad K = \begin{pmatrix} k_1 + k_2 & -k_2 \\ -k_2 & k_2 \end{pmatrix}; \quad (31)$$

Eq. (30) is brought to first-order form of Eq. (1) by introducing the variable $x(t) = [y_1(t); y_2(t); \dot{y}_1(t); \dot{y}_2(t)]^T$, from which we obtain

$$\dot{x}(t) = Ax(t); \quad \text{where } A = \begin{pmatrix} 0 & 0 & 1 & 0 \\ 0 & 0 & 0 & 1 \\ -\frac{k_1+k_2}{m_1} & \frac{k_2}{m_1} & 0 & 0 \\ \frac{k_2}{m_2} & -\frac{k_2}{m_2} & 0 & 0 \end{pmatrix}; \quad (32)$$

The initial states are the box centered at $[1; 10; 0; 0]$ with radius $[0; 1; 0; 5; 0; 5; 0; 5]$. The numerical values for the parameters are $m_1 = m_2 = k_2 = 1$ and $k_1 = 10; 000$.

A.3 ISS

The ISS (International Space Station) model was originally presented in [14] and later proposed as a benchmark example for order-reduction techniques [30] and

reachability analysis [4]. It is a structural model of the component 1R (Russian service module) and models the vibration during the docking maneuver of a spacecraft. There are 270 state variables and three nondeterministic inputs. The matrices A and e^A are sparse ($> 99\%$ sparsity) with $\|A\|_\infty \approx 3763$, $\|X_0\|_\infty = 10^{-4}$, and $\|U\|_\infty \approx 0.98$.

B User interface

The methods described in Section 3 have been implemented in the library `ReachabilityAnalysis.jl` in the Julia programming language. The implementation offers a user interface that allows to choose different algorithms that can be used through the `discretize` function. It receives three arguments: an initial-value problem of the form (1) (special cases included), the step size δ , and an algorithm (which defaults to the `Forward` method). The function returns a discrete-time system whose set of initial states is X_0 , and can be obtained from the examples below with the command `initial_states(Di)`.

```

1 # load reachability library
2 using ReachabilityAnalysis
3
4 # state matrix
5 A = [0.0 1; -4π 0]
6
7 # step-size
8 δ = 1e-2
9
10 # initial states (infinity-norm ball)
11 X0 = BallInf([0.0, 10.0], 0.1)
12
13 # initial-value problem
14 P = @ivp(x' = A*x, x(0) ∈ X0)
15
16 # use default discretization (Forward-only)
17 D1 = discretize(P, δ)
18
19 # use first-order ddt discretization
20 D2 = discretize(P, δ, FirstOrderddt())
21
22 # use correction hull with default order (p = 10)
23 D3 = discretize(P, δ, CorrectionHull())
24
25 # use correction hull with specified order (p = 15)
26 D4 = discretize(P, δ, CorrectionHull(order=15))

```

Finally, we mention that the library offers a `solve` function that first calls `discretize` and then uses the desired set propagation algorithm to compute the set of states reachable until a given time horizon. These steps correspond to the first (resp. second) stages according the notation in Section 1. We refer to the online documentation of `ReachabilityAnalysis.jl` for further examples.

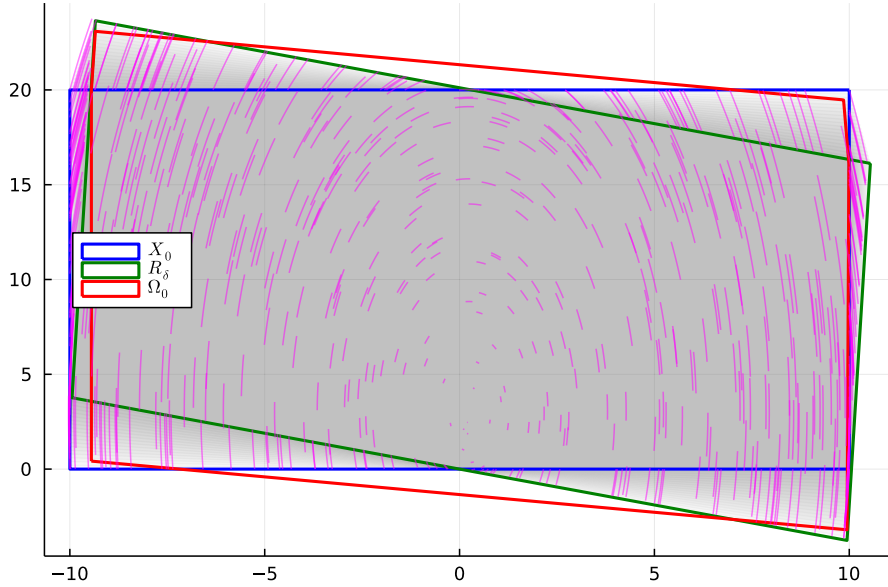


Fig. 7: The set Ω_0 (red) obtained with the “d/dt” method aimed to underapproximate. The system evolves from \mathcal{X}_0 (blue) to $\mathcal{R}(\cdot)$ (green) and the reachable set spans the shape of a bow tie, as can be seen from the trajectories (magenta) and some sets \mathcal{R}_t for uniform $t \in [0; \delta]$ (gray). The set Ω_0 contains the unreachable triangles at the top and bottom.

C Underapproximation

The authors of the “d/dt” method claim that their method can be used to also obtain an underapproximation [10]. Recall the equation (8). Instead of bloating the set $CH(\mathcal{X}_0; \mathcal{X}_0)$, one can also shrink it. The authors originally do this by “inward-pushing” of the constraints of the polytope, but the idea also naturally extends to a support-function representation of the set. Denote this shrinking operator with \ominus . The claim is that the set

$$CH(\mathcal{X}_0; \mathcal{X}_0) \ominus \mathcal{B}_\varepsilon$$

is an underapproximation of the true reachable states. Unfortunately, the error analysis for \ominus only holds for singleton initial states $\mathcal{X}_0 = \{\mathbf{x}_0\}$ and is incorrect for proper sets of initial states. Hence this method does not generally yield a sound underapproximation, which we visualize in Fig. 7.

The problem is that \ominus only takes into account the error for the linear interpolation of \mathbf{x}_0 and \mathbf{x}_1 , for each $\mathbf{x}_0 \in \mathcal{X}_0$; but the convex hull also contains line segments connecting unrelated points \mathbf{x}_0 and \mathbf{x}_1 for $\mathbf{x}_0 \neq \mathbf{x}_1$. This becomes apparent if \mathbf{x}_0 and \mathbf{x}_1 are sufficiently different, i.e., if \mathcal{X}_0 is large, as in the figure.

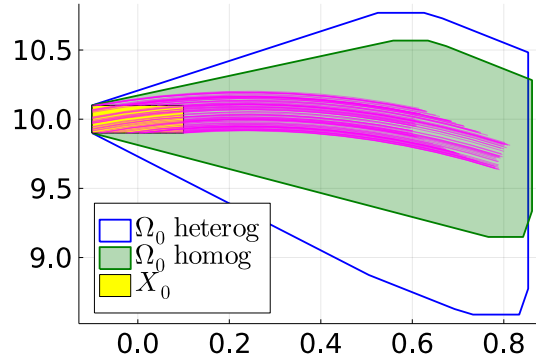


Fig. 8: Several trajectories and the sets Ω_0 obtained with the “forward-only” method for a nondeterministic heterogeneous system and its partial homogenization, projected to the first two dimensions.

Take the point x_0 as the upper right corner and the point x_1 as the upper left corner. The line segment is the upper edge of the red shape in the figure, which is pushed inward but still falls outside the reachable states.

D Homogenization for nondeterministic systems

Fig. 8 shows the effect of partially homogenizing a nondeterministic system as described in Section 4.1. It is observed that homogenizing the system improves the precision of the resulting set.